2.7 CRACK HEALING BY ANNEALING IN 14YWT NANOSTRUCTURED FERRITIC ALLOY, FCRD NFA-1 — M.E. Alam, S. Pal, G. R. Odette (UCSB), D. T. Hoelzer (ORNL) and S. A. Maloy (LANL)

OBJECTIVE

The objective of this study is to explore the effects of annealing on the microstructural and mechanical properties of a newly developed larger best practice heat of 14YWT nanostructured ferritic alloy, NFA-1.

SUMMARY

FCRD NFA-1 is a new 14YWT nanostructured ferritic alloy (NFA) processed to form a 12.5 mm thick plate. Plane sections parallel to the broad plate surface have a nearly equiaxed, ultrafine grain structure. In contrast, the plane sections parallel to the narrow plate thickness side contain pancake shaped grains with a tri-modal size distribution, including some that are very large, and a population of microcracks running normal to the thickness direction. At 23°C tensile specimens loaded in the short thickness direction have flat, faceted fracture surfaces and no ductility due to cleavage initiation of the microcracks. The corresponding tensile ductility increases with test temperature due to a brittle to ductile transition near about ~150°C. Annealing at 1300°C/1h appears to heal the microcracks, resulting in ductile fracture for short thickness direction axis loading. Annealing also appears to alter the grains and reduces the room temperature (23°C) yield stress by ≈ 13%. Tensile tests at 600°C showed relatively isotropic properties in both conditions, and a smaller reduction in strength following annealing.

PROGRESS AND STATUS

Materials and Methods

The nanostructured ferritic alloys (NFAs) are a promising candidate alloy class for the advanced nuclear fission and future fusion reactor applications, since they have high tensile, fatigue and creep strengths over a wide range of temperature, as well as unique irradiation tolerance and outstanding thermal stability up to 1000°C. These attributes derive from the presence of submicron size grains, high dislocation densities and especially an ultrahigh population of nanometer size Y-Ti-O rich multifunctional nano-oxides (NO) [1]. NFA-1 was developed in collaboration between UCSB, ORNL and LANL to explore including Y in the Fe-14Cr-3W-0.4Ti-0.2Y melt prior to gas atomization by ATI Powder Metals (Pittsburgh, PA). However, the Y was phase separated after atomization. Thus a low interstitial alloy powder (15 kg) variant was ball milled for 40 hours with FeO (52.5 g) to increase the O content and to mechanically alloy the Y into solution. The milling was carried out by Zoz GmbH (Wenden, Germany) using a CM100b attritor mill with a ball mass-to-charge ratio of 10:1 and ball size of 5 mm. The milled powders were then consolidated at ORNL by hot extrusion at 850°C. The extruded bar was annealed for 1 hour and then hot cross-rolled to a ≈ 50% thickness reduction, both at 1000°C, to produce an ≈ 12.5 mm thick plate [2]. The as-fabricated plate has been extensively characterized as reported elsewhere [3]. Tensile specimens extracted from the plate wrapped in a molybdenum getter foil were annealed in a low pressure Ar environment at 1300°C for 1 h.

The as fabricated and annealed NFA-1 conditions were characterized using a scanning electron microscope (SEM) equipped with energy dispersive spectroscopy (EDS) and electron backscatter diffraction (EBSD) detectors. The tensile specimens were ground (to 1500 grit) and polished (to 20 nm colloidal silica), then etched with Kroll's reagent (92% distilled water, 6% nitric acid and 2% hydrofluoric acid) prior to examination in a FEI x30, Netherland SEM. Longest (l) and shortest (s) individual grain dimensions were tabulated from the SEM micrographs using 'ImageJ64' software. The effective grain diameter was taken as d = (l+s)/2 and the aspect ratio as r = l/s. EBSD was used to characterize the texture in the plate induced by hot extrusion and cross rolling. Vickers microhardness measurements were performed on polished coupon surfaces at a 500g load using LECO M-400A semi-automated hardness tester, based on the average of 10 to 15 indents. Tensile tests were performed on flat dog-bone shaped sub-sized specimens with a gage section length, width and thickness of 5.0x1.2x0.5 mm^3. The

tensile tests were performed for longitudinal (L), transverse (T) and short (S) thickness directions as illustrated in Figure 1, at both room temperature and 600°C, on a 810 MTS servo-hydraulic universal testing machine equipped with a clam shell furnace. The tensile specimens were sanded with 1500 grit to remove surface contamination, minor defects and local residual stresses due to the EDM used to fabricate them. The specimens were heated to the target temperature in atmosphere, and held for 10 minutes before testing. Loading was carried out at a crosshead speed of 0.30 mm/min, or a strain rate of $\approx 10^{-3}$/s. Except for the small size of the specimens, the tensile properties were determined in accordance with ASTM Standard E8M-13. The fracture surfaces of the broken tensile specimens were extensively characterized by SEM.

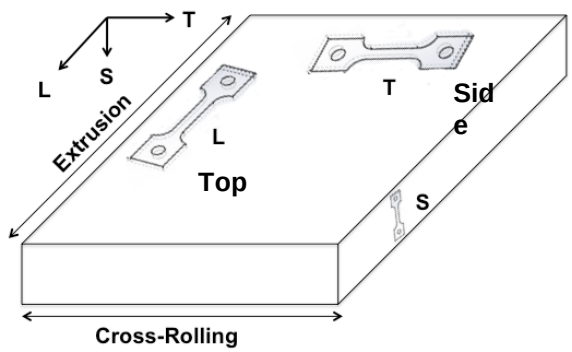

Figure 1. NFA-1 specimen orientations labeled with respect to the extrusion, cross-rolling and plate thickness directions.

Results and Discussion

- Microstructure

Figs. 2a and d show SEM micrographs of the plate normal (L-T or top) view with nearly equiaxed, unimodal and ultrafine grains, in both the as fabricated and 1300°C annealed conditions. The grains are ≈ 20% larger following annealing. Figs. 2b and c show that the as-fabricated L-S (side) plane contains a number of microcracks running on planes normal to the plate thickness direction. The corresponding grains are elongated and pancake-shaped with a tri-modal grain size distribution (many < 1 µm, some 1-10 µm and a few very large grains). As shown in Figs. 2e and f, microcracks are not observed in the L-S (side) view of the annealed specimens. Both the corresponding grain size and aspect ratio appear slightly smaller in the annealed versus as-fabricated condition. An EDS scan indicates the presence of Ti-rich precipitates in stringers along the extrusion direction. High temperature annealing appears to heal the cracks, presumably by surface diffusion, perhaps assisted by recrystallization and grain boundary migration [4].

Table 1. Grain morphology and microhardness of as-fabricated and 1300°C annealed NFA1

Location, Condition	Grain Size (nm)	Aspect Ratio	Microhardness (Hv)
Top, as-fabricated	454 ± 142	1.2 ± 0.2	376 ± 18
Side, as-fabricated	(1077 ± 509) x (397 ± 124)	2.7 ± 1.1	352 ± 39
Top, annealed	705 ± 346	1.2 ± 0.4	294 ± 13
Side, annealed	(822 ± 516) x (341 ± 115)	2.4 ± 1.4	304 ± 17

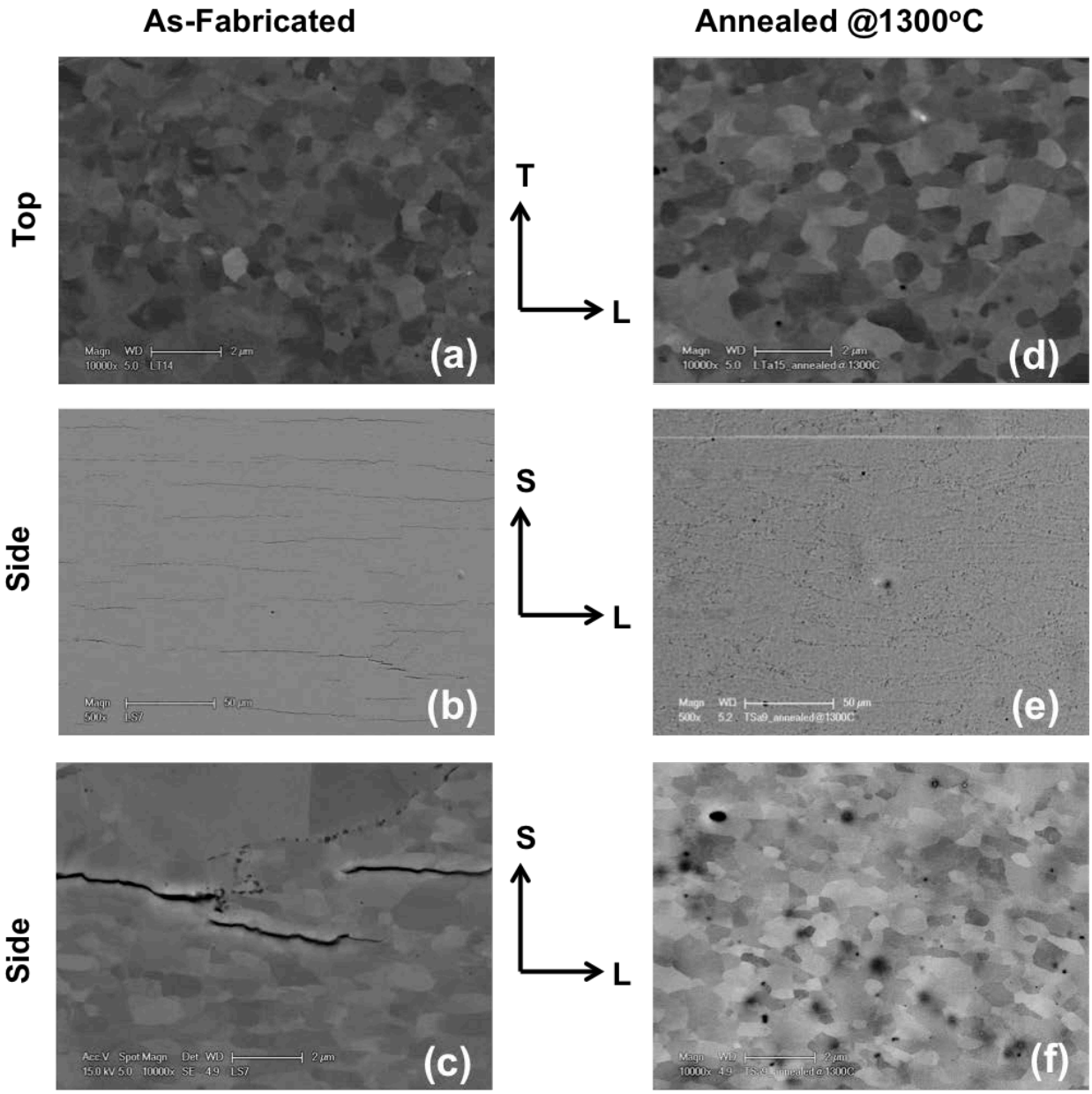

Figure 2. SEM images showing plate's: a) top; b and c, side view morphology, respectively, for as-fabricated (left) and 1300°C annealed samples (right).

Figure 3 shows inverse pole figure (IPF) maps for as-fabricated and annealed conditions with both top and side views measured using EBSD techniques. Subgrains and grains were characterized by means of misorientation angle distribution (MAD) measured using EBSD. A misorientation angles greater than 3° (red) and less than 15° is considered as subgrain boundary, while, above 15° (black) it is taken as a grain boundary.. Consistent with the SEM observations, Figure 3a shows small and nearly equiaxed grains in the plate's L-T (top) view, while Figure 3b shows larger and grains elongated in the extrusion direction in the side views in the as-fabricated condition. Some very large and highly elongated grains are also observed, including one in the vicinity of a microcrack. Low angle grain boundaries are found inside the larger grains (marked as red). The IPF maps highlight the strong preferential crystallographic orientation

of most of the grains with a <110> direction parallel along with the extrusion directions. As shown elsewhere [5], the texturing is accompanied by the development of (100) planes normal to the thickness direction, thus creating a corresponding (100)<110> texture component, which is the most brittle cleavage system for bcc Fe. In combination with stress concentrations, this leads to the formation of the population of microcracks. In contrast, the side view of the annealed condition is crack-free, relatively equiaxed and nontextured with a bimodal grain distribution as seen in Figure 3d.

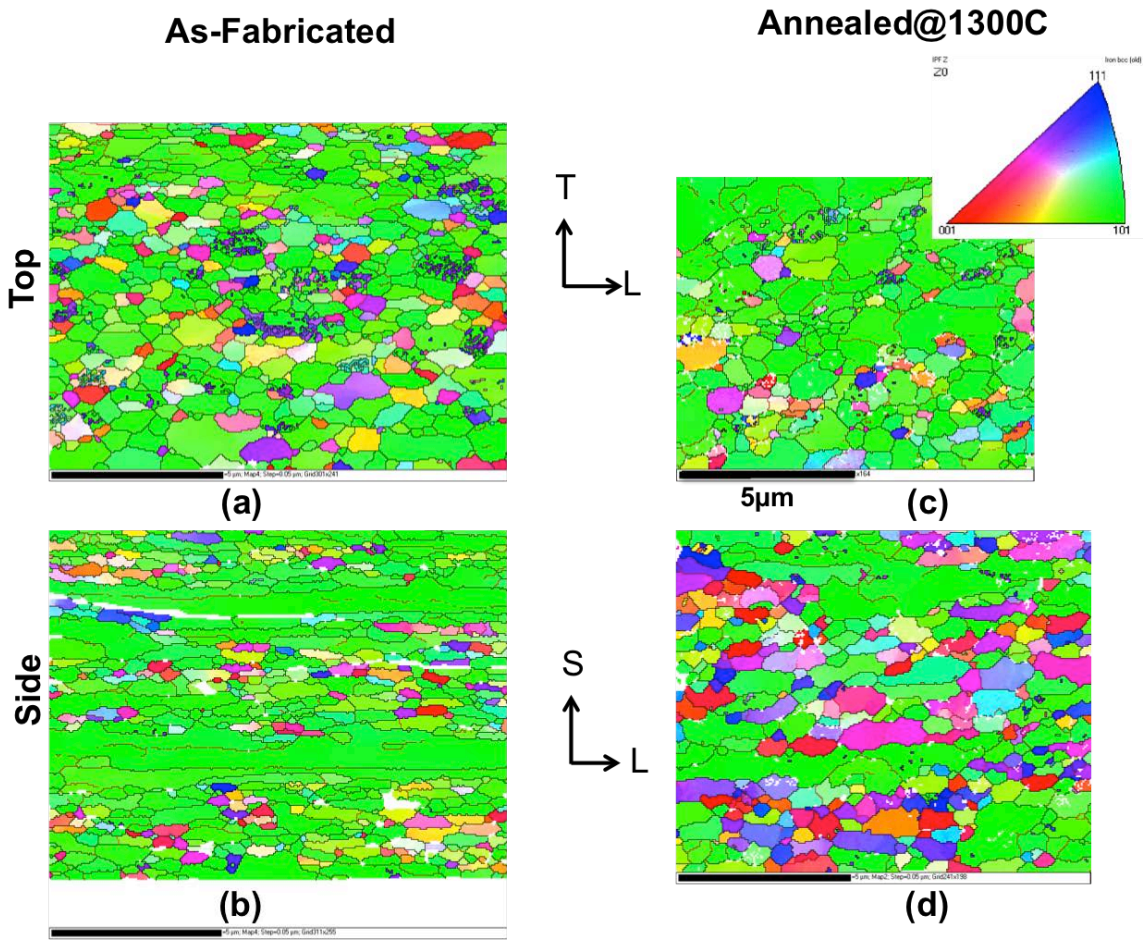

Figure 3. IPF maps obtained by EBSD for the as-fabricated condition (left) with a) top and b) side views; the corresponding IPF map for the annealed condition (right) with c) top and d) side views.

Microhardness

Vicker's microhardness (H_v) data for the NFA-1 are also summarized in Table 1. For the as-fabricated condition H_v averages 376 ± 18 (kg/mm^2) for the top surface and 352 ± 39 (kg/mm^2) for the side surface for specimens. These differences can probably be attributed to some coarsening of the NO and grains. The lower H_v and higher standard deviation for the side surface might be due to softening associated with delamination. The H_v is lower after annealing and similar for the two surfaces, with smaller standard deviations.

Tensile Properties

Figure 4 shows engineering stress-strain s(e) curves from room temperature tensile tests in the three L, T and S orientations (see Figure 1), for both the as-fabricated and annealed conditions. The as-fabricated L and T orientations have similar s(e), with 0.2% yield stress (YS) and ultimate tensile strength (UTS) values varying from 951-961 MPa and 1062-1082 MPa, respectively. The total elongations range from 12.8 to 15.3%. In contrast, the as-fabricated S orientation has the lowest strength with YS = UTS = 652 MPa, fracturing in the elastic region, without any plastic strain. The s(e) for the L and T oriented annealed condition are also similar to each other, with ≈ 14% lower strength than the as-fabricated condition. While the as-fabricated S oriented tensile specimen failed in the elastic region at room temperature, the corresponding annealed condition has a large total elongation of ≈ 18%, with slightly higher YS ≈ 700 MPa and a significantly higher UTS of ≈ 874 MPa compared to the as fabricated condition. The strength and ductility for annealed condition in the S orientation is comparable to the annealed L and T oriented specimens. These improvements in strength and ductility are associated with the absence of microcracks (Table 1 and Figure 2). The lower YS in this case is due to a lower stress marking the deviation from the elastic loading line. But this may be an experimental artifact since all three orientations have otherwise very similar s(e) curves.

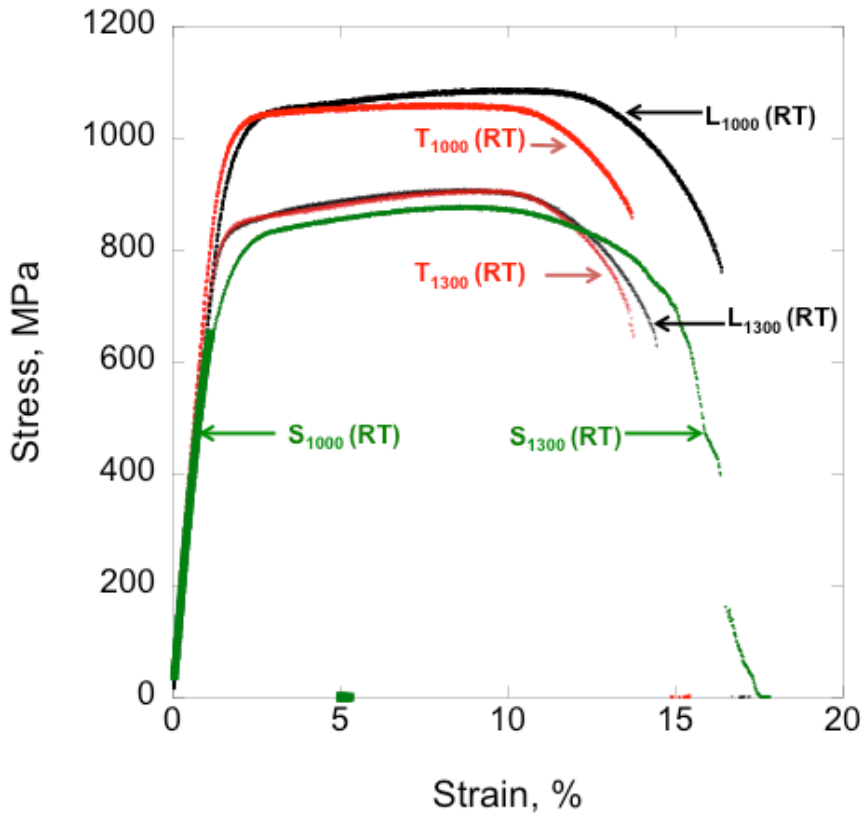

Figure 4. Room temperature engineering stress-strain curves of as-fabricated (1000°C) and annealed (1300°C) NFA-1 specimens tested in three different orientations.

Figures 5 and 6 show the fracture surfaces of the broken tensile specimens. Delaminations occurred in both the as-fabricated condition L and T specimens normal to the thickness direction in planes parallel to the plate surfaces. In contrast, the annealed condition is delamination-free. Again the fracture surface is

flat and brittle for the S orientation in the as-fabricated condition, in contrast to fully ductile fracture in the annealed condition. Corresponding higher magnification images in Figure 6 show ductile dimples in all the annealed specimen along with shallow crater-like features, which might be partly responsible for lower strength along with higher grain size compared to the as-fabricated specimens. The crater like features may partially healed microcracks.

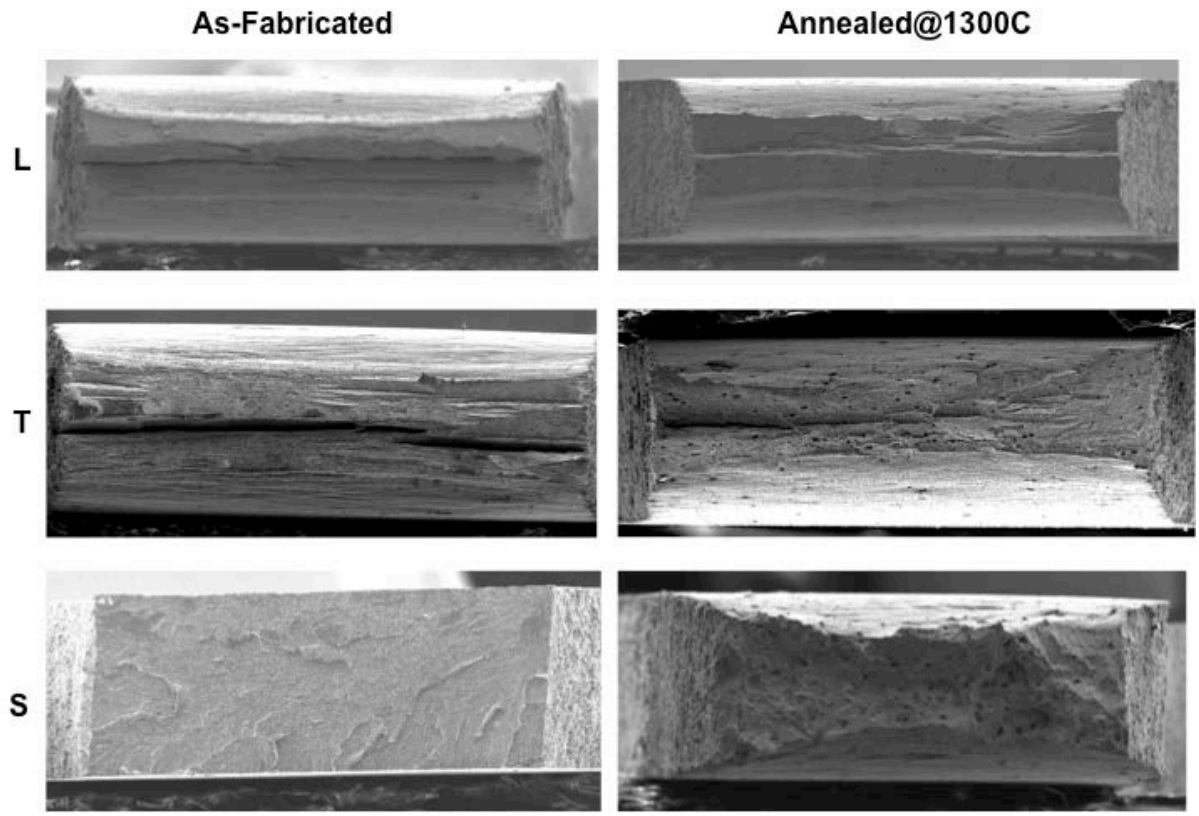

Figure 5. Low magnification SEM fractographs of room temperature as-fabricated and annealed tensile fracture surfaces for different orientations.

Figure 7a shows the s(e) for tensile test on annealed T and S oriented specimens at 600°C. Both the strength (YS and UTS) and ductility decrease at higher temperature. In both cases, the uniform elongations are quite low (~1.3%) compared to at room temperature (7-8%). However, the annealed specimens retained significant strength levels of YS = 432-489 MPa and UTS = 469-502 MPa, and ductility, with total elongation strains of 9-10%. This compares to corresponding as-fabricated strength and ductility values of YS ≈ 484-547 MPa, UTS ≈ 529-580 and total elongation strains of 13.5-14.4%. As seen in Figure 7b, no delaminations are observed in the annealed condition. Relatively flat fracture surfaces were observed for both T and S orientations with reductions in area of ≈31% and ≈12%, respectively. Higher magnification SEM images in Figure 7b, show dimples associated with coarser oxide particles in both cases, along with crater-like features. However, the dimples for the S orientation appear to be composed of larger and smaller features. The larger features are filled with small dimples on their sidewalls. Note the surfaces are oxidized during high temperature testing. In the annealed condition L, T and S orientations strength and ductility values are comparable both for the room temperature and 600°C tests. Thus NFA-1 exhibits nearly isotropic behavior when annealed at 1300°C.

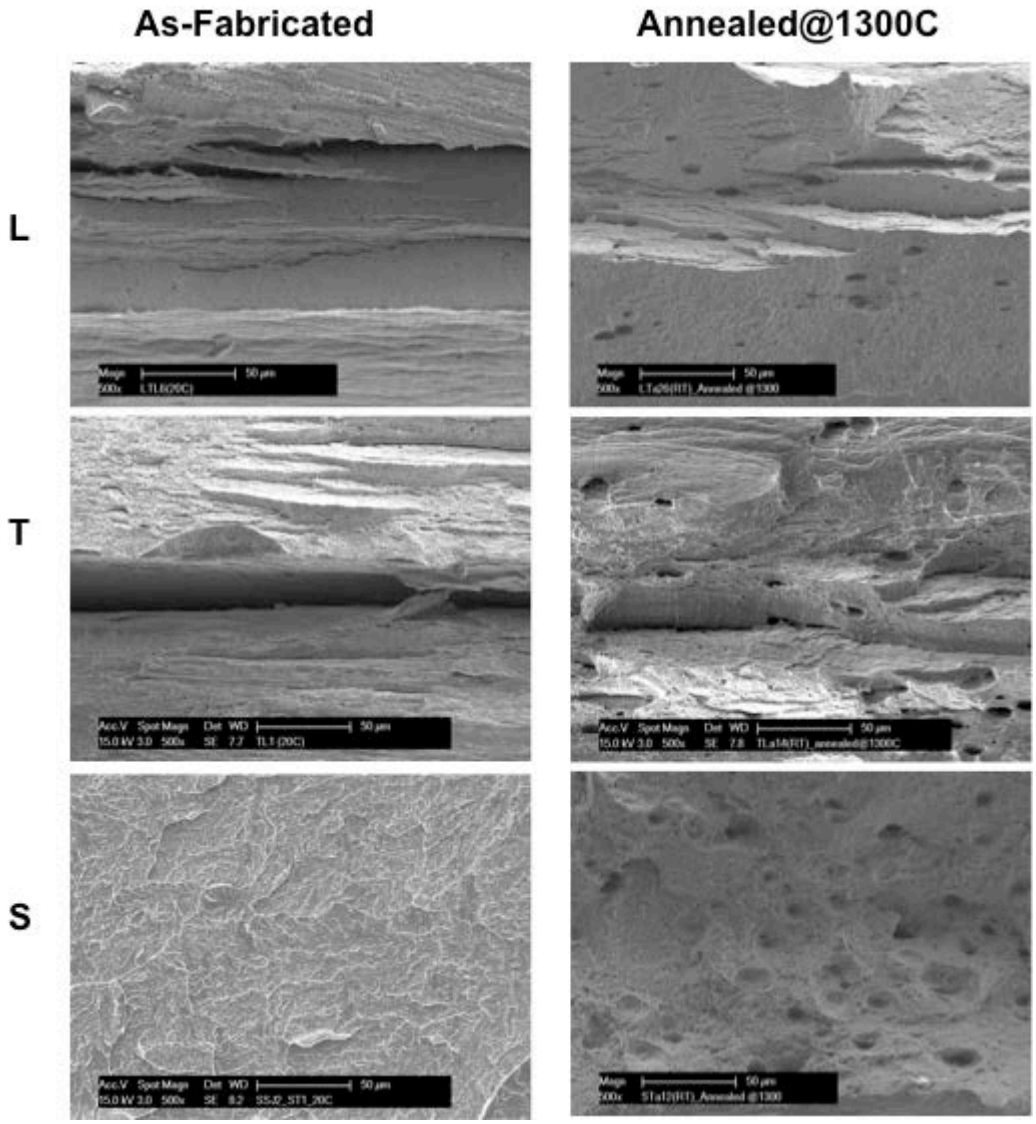

Figure 6. High magnification SEM fractographs of room temperature as-fabricated and annealed tensile fracture surfaces at different orientations.

Summary and Future Work

The effect of annealing 1300°C for 1 h on as-fabricated NFA-1 was characterized in terms of grain structures, microcracks, microhardness and tensile properties. High temperature annealing appears heal the microcracks that exist in the as-fabricated plate. Annealing also increases the average grain size by ≈ 20% reduces both the microhardness by ≈ 18% and room temperature tensile YS and UTS by ≈ 13% lower. The room temperature tensile properties are more isotropic after annealing.

The effect of different annealing temperatures and times will be explored and more detailed observations on microcrack healing will be carried out along with the corresponding effects on the grain, dislocation and NO nanostructures will be characterized. Mechanical property measurements will be extended to fracture toughness.

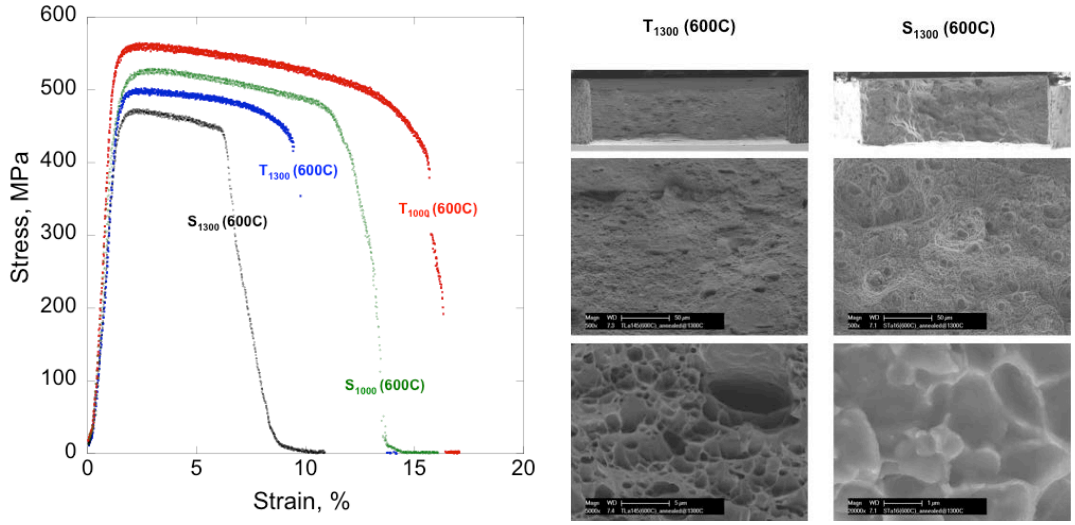

(a) (b)

Figure 7. a) Engineering stress-strain curves of annealed specimens tested at 600°C, and b) their SEM fractographs.

Acknowledgments

This work is part of a multi-laboratory collaboration between LANL, UCSB and ORNL. The DOE Office of Fusion Energy Sciences supported some of the mechanical testing reported here. NFA-1 was produced under the sponsorship of the DOE Office of Nuclear Energy through both a NEUP grant and the FCRD program.

References

[1] G.R. Odette, "Recent progress in developing and qualifying nanostructured ferritic alloys for advanced fission and fusion applications," JOM. 66 (2014) 2427.

[2] N.J. Cunningham, Y. Wu, G.R. Odette, D.T. Hoelzer, S.A. Maloy, " Characterization of a larger best practice heat of 14YWT in annealed powder, HIP consolidated and extruded forms", Fusion Materials Semiannual Progress Report for Period Ending June 30, 2013, DOE/ER-0313/54, U. S. Department of Energy, 15.

[3] M.E. Alam, K. Fields, G. R. Odette, D. T. Hoelzer and S. A. Maloy, "Tensile property characterization of 14YWT nanostructured ferritic alloy NFA1" Fusion Materials Semiannual Progress Report for Period Ending December 31, 2014, DOE/ER-0313/57, U. S. Department of Energy, 39.

[4] K.W. Gao, L.J. Qiao, and W. Y. Chu, "In situ TEM observation of crack healing in α-Fe", Scripta Materialia, 44 (2001) 1055.

[5] A. G. Junceda, M. H. Mayoral and M. Serrano, " Influence of the microstructure on the tensile and impact properties of a 14Cr ODS steel bar", Materials Science and Engineering A, 556 (2012) 696.